Part II

ACTIVE MEDIA

Chapter 6

Random amplifying media

6.1 Introduction

In the early fifties, the field of Optics regenerated a lot of excitement owing to the successful operation of the ammonia maser by Gordon, Zeiger and Townes[1]. This remarkable development was carried forward into the optical regime by Maiman[2], when he obtained oscillation at a wavelength of 693.4 nm, using a ruby crystal. Stimulated emission with resonant feedback was shown to result in light output of very high intensities. Beginning with that crude design of an amplifier, lasers have come a long way with extreme sophistication due to various technological advances[3]. The skeletal design of the laser , i.e. mirrors enclosing an amplifying medium is shown in figure 6.1, which depicts a flashlamp pumped laser. The amplifying medium absorbs the light energy emitted by the flashlamp, and stores this energy in the form of inverted population. Photons emitted spontaneously from the medium exit the medium in all possible directions, and those which are emitted along the axis of the resonator are reflected back into the amplifying medium. These reflected photons, then, stimulate the atoms of the medium to emit light, and the stimulated emission has the same properties as that of the stimulating photons. This process, called gain, depends upon the pathlength of a photon inside the excited medium, and goes as $\sim exp(\alpha l)$, where a is the gain per unit length, and l is pathlength inside the excited medium. The two reflectors on either side of the amplifying medium repeatedly reflect

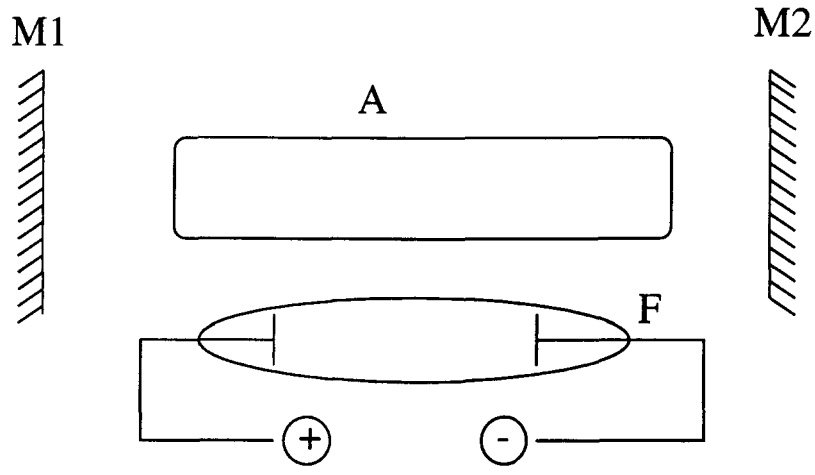

Figure 6.1: *A skeletal design of a laser, here, a flashlamp pumped laser. A : Amplifying medium, F : Flashlamp, M1 and M2 : Mirrors.*

the photons into the amplifying medium, and thus increase the pathlength, and consequently the gain, resulting into lasing action. This basic design has remained unchanged over the years, and any modification in the device has been only in the amplifying media, the pumping mechanism, the Q-switching devices, phase plates leading to different modes of the laser beam etc. The shape of the resonators is also modified in a few cases so as to enhance the efficiency of pumping. However, the condition of resonant feedback is not compromised with at any cost. Though the name *Light Amplification* by *Stimulated Emission of Radiation (LASER)* makes no mention of coherence or directionality, these two properties, which are artefacts of the resonator, have been accepted as the identifying properties of a laser.

At around the same time, in the late sixties, an attempt was made to study the process of lasing with non-resonant feedback involving theoretical treatments and a few experimental investigations[4, 5]. The experiments involved the replacement of one of the mirrors of the resonator by a scattering surface. Consequently, all the individual high-Q resonances seen with resonant feedback are replaced by a number of overlapping low-Q resonances. These low-Q resonances overlap and form a continuous spectrum. As a result, the spectrum of the emission generated tends to be continuous, and does not contain

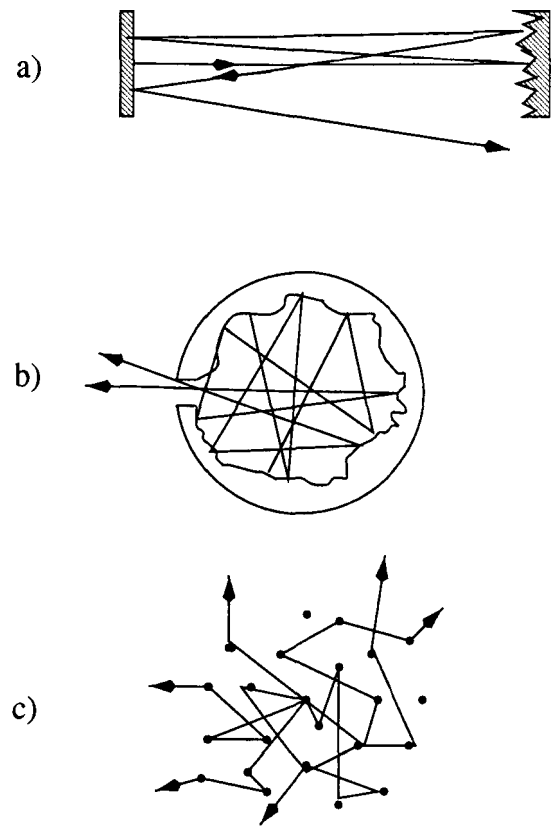

Figure 6.2: *Different designs of cavities with non-resonant feedback. a) a mirror and a scattering surface, b) cavity with scattering walls and an outlet hole and c) scattering particles in an amplifying medium. In all these three cases, light follows tortuous paths before exiting the region of excitation.*

discrete components at selected resonant frequencies. The only resonant element that remains, then, is the gain profile of the amplifying medium. Therefore, after crossing the threshold, the spectrum narrows continuously towards the maximum of the gain profile. In that experimental report, it was found that spectral narrowing is much slower than in ordinary lasers. Further, as is understandable, the narrowed output had no spatial and temporal coherences as compared to the resonant laser. Since directionality and coherence are the two most characteristic features of a laser, the above findings did not create much interest in the application of non-resonant feedback to achieve lasing action.

A scattering-amplifying system different from the one described above was treated theoretically in details by Letokhov in 1968[6]. This system involved both scattering

and amplification in the same region of space. Such a scattering-amplifying system was studied experimentally[7] using the powdered crystals of Eu^{2+}. In this case, the particles of the amplifying material themselves acted as the scatterers. It was only recently in the year 1994 that Lawandy et al[8] reported laser-like emission from an amplifying medium that was doped with scattering particles. In this case, the light got amplified between two scattering events. The amplifying medium used was a laser dye Rhodamine 640 perchlorate dissolved in methanol, and the scatterers were TiO_2 microparticles. This dye-scatterer combination carries an advantage that one has a free handle on various parameters like the gain coefficient, scattering strength etc. When the pure dye was pumped using pulses of NdYAG laser ($\lambda = 532$ nm), the spectral width of the emissions from the dye was seen to narrow down to about 4 nm from its normal width of about 40 nm. The pump energy at which this happened, called the threshold, was seen to lower down drastically with the addition of scatterers. This was attributed to laser action due to non-resonant feedback. The pathlength of the photons in the medium were increased due to multiple scattering off the microparticles. Since the gain is proportional to the pathlength ($\sim exp(\alpha l)$), multiple scattering resulted in generation of light with narrow linewidth and high intensity. The experiment generated a lot of interest that has resulted in extensive experimental and theoretical research in the field of lasers using non-resonant feedback[9-21]. The system of amplifying medium and scattering particles has been termed "mirrorless lasers" for obvious reasons[22]. Since the amplifying media in such systems are disordered or have a random refractive index, they have been named as "random lasers". The emissions from such systems are devoid of any coherences or directionality. It is still being debated whether the emissions from such media are really a result of lasing, or merely amplified spontaneous emission.

For a system to be called a laser, temporal coherence is a necessary feature in its emissions. The dye-scatterer system does not exhibit any temporal coherence due to the random positions of the scatterers which rule out any mode selection through resonant oscillations inside the amplifying medium. It was believed that any scattering system that

was strong enough to localise light would give rise to resonances due to closed loop paths inside the scattering medium[22]. Such a path, in the presence of amplification, would lead to a temporally coherent emission, albeit in random direction. After the first experimental report of localisation of light[23], a group from Illinois reported their experimental results from the study of a scattering-amplifying medium that was capable of localising light[24]. They did show that the emission had large temporal coherence. This is perhaps the first random laser, in the true sense of the word. The simplicity of its structure and minimal pumping requirements make a random laser a strong candidate to replace the conventional laser, at least as an intense, narrowband light source. Size requirements for such a source are also minimal. A microlaser based on disordered amplifying media has been demonstrated to have the size of a micrometer-scale[25]. Localisation of light in such a microlaser narrows the emission linewidth to 0.09nm.

6.2 The dye-scatterer system

After the report of Lawandy et al, the system of dye and scatterers has been studied in fine detail, pertaining to the change in its spectral and temporal characteristics upon addition of scatterers. Numerous researchers have examined various combinations of different dyes and scatterers, with or without external feedback, under different pumping geometries. Reports from these experiments have prompted theories of random lasing based upon light diffusion with gain[13, 15] or sub-diffusion scattering with high gain[16] depending upon the strength of scattering. Anderson's localisation of light has not yet been reported in such a system because of the small refractive index of scatterers at the wavelength of emission of the dyes.

We introduce the dye-scatterer system used in our experiments.

Laser dyes such as Rhodamine 6G, Rhodamine B or Rhodamine 640 perchlorate dissolved in suitable solvents are used as the amplifying material. These dyes are used in conventional dye lasers due to their high quantum efficiency.

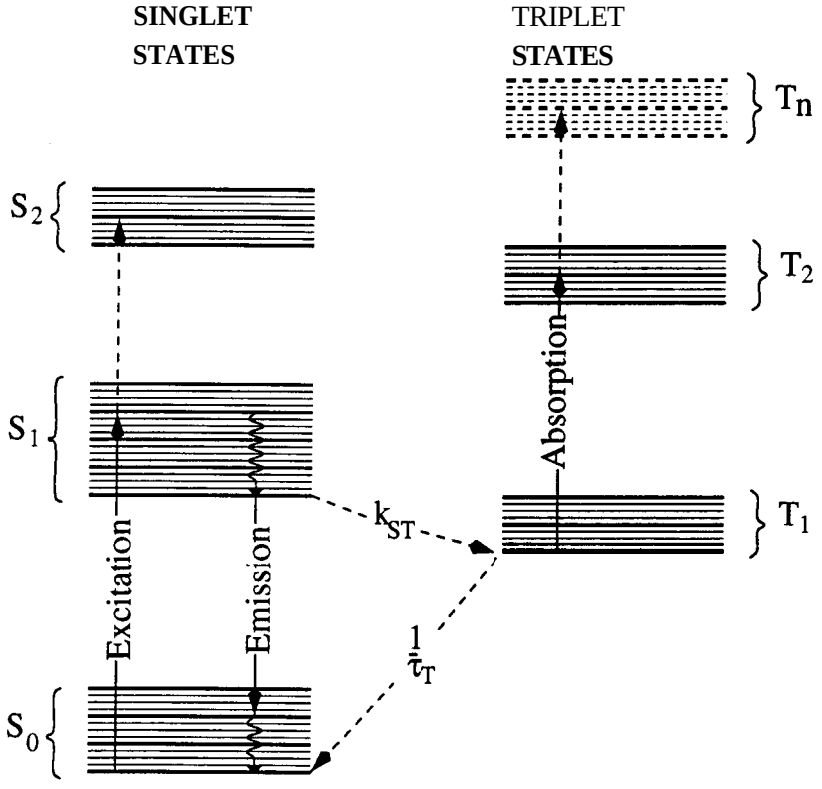

Figure **6.3:** *Schematic energy level diagram for a dye molecule. The processes of importance in the operation of a dye laser are shown by arrows. The bold horizontal lines represent vibrational sublevels of the electronic states and the lighter lines represent levels due to interaction of the dye molecule with a solvent. Various processes involved are explained in the text.*

Typical energy level diagram[26] of a dye molecule dissolved in solvent is shown in figure 6.3. There is a ladder of singlet states $S_i(i = 0, 1, 2...)$, the lowest of which is the ground state. There is another ladder of triplet states, somewhat displaced towards lower energies $T_i(\mathrm{i} = 1, 2, 3...)$. Absorption of suitable energies pumps the molecule from the ground state to S_1 or S_2 etc. The radiative transition from singlet states to the triplet states is forbidden and can occur only through non-radiative means via internal and external perturbations. These transitions are called intersystem crossings and take place at the timescale of 10 nanoseconds. The decay from the higher singlet states to the S_1 state is also non-radiative, and takes place at the timescale of a picosecond. The decay from the lowest triplet state to the ground state is radiative, and is called phosphorescence. This transition occurs at the timescale of a microsecond. Since this transition is very slow, the lowest triplet state is called the trapping state. The efficiency of the radiative processes is reduced if this state starts getting populated. Transitions like $T_1 \rightarrow T_n$ (triplet-triplet) are also allowed, and the molecules in the higher triplet states decay to T_1 non-radiatively followed by phosphorescence to the ground state.

The only process of interest to us is the fluorescence process, which is the decay from the S_1 state to the ground state S_0. When the decay is spontaneous, it occurs at the timescale of one nanosecond and this lifetime is connected to the Einstein coefficient for spontaneous emission. When a molecule absorbs energy, it is transferred from the S_0 state to one of the vibronic sublevels of the S_1 state. The availability of a large number of such vibronic sublevels explains the broad absorption band of such dyes. The excited molecule cascades down to the lowest vibronic sublevel of S_1, and therefrom, fluoresces to one of the vibronic sublevels of S_0. Once again, the availability of the vibronic sublevels in the S_0 state gives rise to the broad emission band of the dye molecules.

Since the energy bands of the dye molecule is modified because of its interaction with the solvent molecules, the same dye can, when dissolved in different solvents, exhibit significantly different emission properties. This has been traced to the dipole moment of the solvent molecules, the relative acidity of the solvent and the dye molecules etc. Apart

Typical energy level diagram[26] of a dye molecule dissolved in solvent is shown in figure 6.3. There is a ladder of singlet states $S_i(i = 0, 1, 2...)$, the lowest of which is the ground state. There is another ladder of triplet states, somewhat displaced towards lower energies T_i(i $= 1, 2, 3...$). Absorption of suitable energies pumps the molecule from the ground state to S_1 or S_2 etc. The radiative transition from singlet states to the triplet states is forbidden and can occur only through non-radiative means via internal and external perturbations. These transitions are called intersystem crossings and take place at the timescale of 10 nanoseconds. The decay from the higher singlet states to the S_1 state is also non-radiative, and takes place at the timescale of a picosecond. The decay from the lowest triplet state to the ground state is radiative, and is called phosphorescence. This transition occurs at the timescale of a microsecond. Since this transition is very slow, the lowest triplet state is called the trapping state. The efficiency of the radiative processes is reduced if this state starts getting populated. Transitions like $T_1 \rightarrow T_n$ (triplet-triplet) are also allowed, and the molecules in the higher triplet states decay to T_1 non-radiatively followed by phosphorescence to the ground state.

The only process of interest to us is the fluorescence process, which is the decay from the S_1 state to the ground state S_0. When the decay is spontaneous, it occurs at the timescale of one nanosecond and this lifetime is connected to the Einstein coefficient for spontaneous emission. When a molecule absorbs energy, it is transferred from the S_0 state to one of the vibronic sublevels of the S_1 state. The availability of a large number of such vibronic sublevels explains the broad absorption band of such dyes. The excited molecule cascades down to the lowest vibronic sublevel of S_1, and therefrom, fluoresces to one of the vibronic sublevels of S_0. Once again, the availability of the vibronic sublevels in the S_0 state gives rise to the broad emission band of the dye molecules.

Since the energy bands of the dye molecule is modified because of its interaction with the solvent molecules, the same dye can, when dissolved in different solvents, exhibit significantly different emission properties. This has been traced to the dipole moment of the solvent molecules, the relative acidity of the solvent and the dye molecules etc. Apart

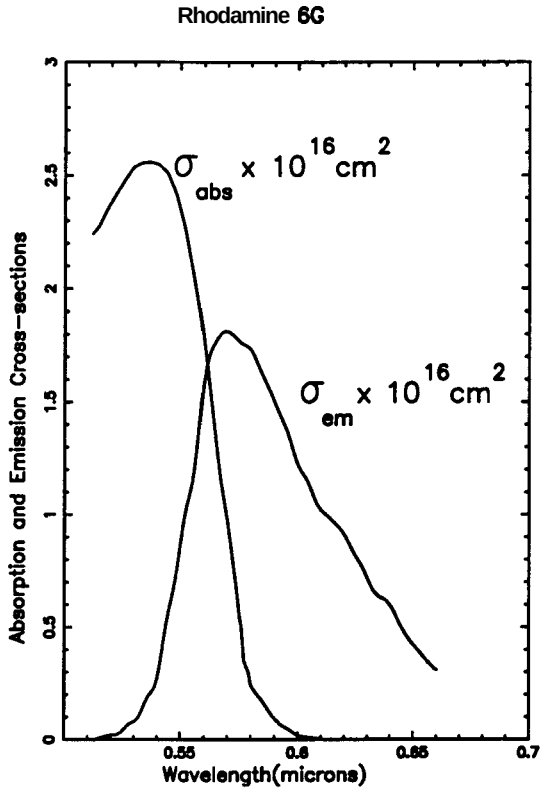

Figure 6.4: *Absorption and Emission cross-sections of the dye Rhodamine 6G, dissolved in water, at a concentration of* $10^{-4}M$.

from the emission profile, the quantum efficiency of the dye is also largely influenced by the solvent.

The figure 6.4 shows the absorption and emission spectra of Rhodamine 6G dissolved in water[26], at a concentration of 10^{-4}M. The absorption cross-section is maximum at 530 nm, which is very close to the wavelength of frequency doubled NdYAG laser. The emission cross-section is largest at around 570 nm. The absorption and emission spectra have a considerable overlap which leads to re-absorption of the fluorescence by the molecules of the dye in the ground state. As a result, the emission spectrum is red-shifted for high concentration dyes.

The scatterers used in our experiments are all polymer particles, spherical in shape, and less than a micron in diameter. In particular, we used two types of microparticles,

polystyrene and polymethylmethacrylate (PMMA). When suspended in ethanol or water, the settling times of these particles are of the order of nanometres per second. Coagulation is prevented because of a coating of a charged surfactant on the particles, which maintains the interparticle separation due to Coulomb repulsion. The absorption by these particles at optical wavelengths is minimal, so the scattering can be assumed to be purely elastic.

6.3 Multiple scattering of light in gain media

As mentioned in the last section, the physical system consists of light wave or photons that scatter elastically off the scattering sites and get amplified during the travel between scattering events. Following parameters are used in describing the physical picture.

The scattering mean free path is the average distance between two scattering events. It is given by

$$l_s = \frac{1}{n\sigma_s} \tag{6.1}$$

Since the scattering mean free path is inadequate to account for the anisotropy in scattering by scatterers larger than the wavelength, we define the transport mean free path l^* as

$$l^* = \frac{l_s}{1-g} \tag{6.2}$$

The anisotropy parameter g $=< cos\theta >$, θ being the scattering angle, accounts for the scattering anisotropy.

To describe the absorption processes, the characteristic lengths used are the inelastic mean free path l_i and the absorption mean free path l_{abs}. The inelastic mean free path l_i is defined as the distance travelled by the wave over which the intensity is reduced to $\frac{1}{e}$ times its initial intensity. The absorption mean free path is the average distance between the begin and end points for paths of length l_i, and is given by

$$labs = \sqrt{\frac{1}{3} l_s l_i} \tag{6.3}$$

When the medium is amplifying, the waves get scattered and amplified as they propagate within the medium. Corresponding to the inelastic length l_i, we define the gain length l_g as the distance over which the intensity of the wave is amplified by a factor of e. The average distance between the begin and end points for this path l_g is called the amplification length, given by

$$l_{amp} = \sqrt{\frac{1}{3} l_s l_g} \tag{6.4}$$

Random lasing has been well-treated by the diffusion theory of light, which assumes that light propagates diffusively inside the gain medium. This approximation works particularly well when l^* is much smaller than the linear dimensions of the sample. The gain is due to the negative absorption coefficient, or the gain coefficient, and the losses are due to the escape of the waves out the surface of the amplifying medium.

The diffusion equation for light transport inside a gain medium is stated as

$$\frac{\partial I(\mathbf{r},t)}{\partial t} = D\nabla^2 I(\mathbf{r},t) + \frac{v}{l_g} I(\mathbf{r},t) \tag{6.5}$$

Here, the second term describes the amplification through l_g, the gain length. v is the transport velocity of the light in the medium.

The amplification of the wave increases as the volume of the amplifying region increases. Loss occurs when the waves escape out of the surface of the amplifying region. Thus, at a certain volume, the gain equals loss, and any more increase in the volume of the medium results in a situation where the intensity diverges. The volume at which the gain becomes equal to the loss is called the critical volume, which for a semi-infinite slab geometry[27], can be expressed as a critical thickness given by $L_{cr} = \pi l_{amp}$, where l_{amp} is the amplification length.

The diffusion theory has largely been used to explain the emissions of a random laser, its temporal characteristics etc[13]. Assuming the pump light also to be diffusive, the

effects of pumping geometry have been studied theoretically[13]. Coherent backscattering from a random amplifying medium has been discussed within the premises of the diffusion approximation[13]. Specific spectral characteristics like bichromaticity of emission have been explained via the diffusion approximation[14].

The diffusion approximation fails to reason the lasing characteristics observed when the linear extent of the gain medium is smaller than the transport mean free path. Indeed, such experimental results have been reported[15]. In that case, an order of magnitude calculation gives the approximate condition of criticality for L << l^* as[16]

$$\frac{W^2 exp(\frac{W}{l_g})}{Ll^*} \geq 1 \tag{6.6}$$

Here, L is the size of the scattering amplifying medium, W is the size of the pumped sub-volume of the total volume. The important condition is the ratio ($\frac{W}{l_g}$), which allows the threshold condition to be realised even for l^* >> L. Noticeably, for large enough l^*, the threshold is missed.

In our studies on passive media, we made extensive use of Monte Carlo simulations in understanding the polarisation aspects of light transport through random media. We employ these techniques in understanding and modelling the phenomenon of random lasing in active random media. Numerical techniques provide a free handle on parameters like pump intensity, strength of scattering etc, and enable us to construct a general model applicable for various different scattering strengths, anisotropies, gain levels etc. The later chapters explain the model that we propose, and also emphasise its generality. This generality, and ease of coding favour the usage of Monte Carlo simulations despite their high cost of computation.

Bibliography

[1] J. P. Gordon, H. Z. Zeiger and C. H. Townes, Phys. Rev. 95, **282 (1954).**

[2] T. H. Maiman, Nature 187, **493 (1960).**

[3] The laser guidebook, J. Hecht, (McGraw-Hill, New York, **1986).**

[4] R. **V.** Ambartsumyan, N. G. Basov, P. G. Kryukov and V. S. Letokhov, JETP Letters 3, **167 (1966).**

[5] **R.** V. Ambartsumyan, N. G. Basov, P. G. Kryukov and V. S. Letokhov, JETP Letters **3, 481 (1966).**

[6] V. S. Letokhov, Sov. Phys. JETP 26, **835 (1968).**

[7] R. L. Fork and D. W. Taylor, Phys. Rev. B 19, 3365 **(1979).**

[8] N. M. Lawandy, R. M. Balachandran, A. S. L. Gomes and E. Sauvain, Nature 368, **436 (1994).**

[9] **W.** L. Sha, C. H. Liu and R. R. Alfano, Optics Letters 19, **1922 (1994).**

[10] **W.** L. Sha, C. H. Liu, Feng Liu and R. R. Alfano, Optics Letters 21, **1277 (1996).**

[11] R. M. Balachandran and N. M. Lawandy, Optics Letters 21, **1603 (1996).**

[12] **R. M.** Balachandran, D. Pacheco and N. M. Lawandy, App. Opt. 35, **640 (1996).**

[13] Diederik Wiersma and Ad Lagendijk, Phys. Rev. E 54, **4256 (1996).**

[14] Diederik Wiersma, Meint P. van Albada and Ad Lagendijk, Phys. Rev. Lett. 75, **1739 (1995).**

[15] Sajeev John and Gendi Pang, Phys. Rev. A 54, **3642 (1996).**

[16] B. Raghavendra Prasad, Hema Ramachandran, Ajay Kurnar Sood, C. K. Subramanian and N. Kumar, App. Opt. 36, **7718 (1997).**

[17] G. A. Berger, M. Kempe and A. Z. Genack, Phys. Rev. E 56, **6118 (1997).**

[18] K. Totsuka, M. A. I. Talukder, M. Matsumoto and M. Tomita, Phys. Rev. B 59, **50 (1999).**

[19] P. C. de Oliveira, J. A. McGreevy, N. M. Lawandy, Optics Letters 22, **895 (1997).**

[20] M. Siddique, R. R. Alfano, G. A. Berger, M. Kempe and A. Z. Genack, Optics Letters 21, **450 (1996).**

[21] D. Zhang, B. Cheng, J. Yang, Y. Zhang, W. Hu and Z. Li, Optics Communications 118, **462 (1995).**

[22] P. Pradhan and N. Kumar, Phys. Rev. B 50, **9644 (1994).**

[23] D. S. Wiersma, P. Bartolini, A. Lagendijk, and R. Righini, Nature 390, **671 (1997).**

[24] H. Cao, **Y.** G. Zhao, S. T. Ho, E. W. Seelig, Q. H. Wang and R. P. H. Chang, Phys. Rev. Lett. 82, **2278 (1999).**

[25] H. Cao, **J.** Y. Xu, E. W. Seelig and R. P. H. Chang, Appl. Phys. Letters 76, **2979 (2000).**

[26] **B. B.** Snavely, Dye Lasers, (Springer-Verlag, Berlin, **1973).**

[27] B. Davison and J. B. Sykes, Neutron Transport Theory, (Oxford University Press. Oxford, **1958).**

Chapter 7

Spectral features of random lasers

7.1 Introduction

Lasing in random amplifying media has been a topic of considerable interest over the last few years. Following the theoretical considerations put forth by Letokhov[1] in 1968, it was experimentally investigated on powdered luminescent samples[2]. In 1994[3], Lawandy et al reported linewidth collapse at reduced thresholds in Rhodamine 6G dye solution on the addition of submicron sized TiO_2 particles. Thereafter, several other groups have reported similar results in various dye scatterer systems[4-8]. There have even been reports of thousand-fold increase in peak emission intensity on the addition of scatterers[8]. This phenomenon has been theoretically studied as diffusion of light due to the random multiple scattering of photons in a disordered medium with gain[9, 10]. The problem was approached numerically by Berger et al[11] where they studied a Monte Carlo simulation of the random walk of photons, assuming isotropic scattering of photons within the gain medium. This is equivalent to solving the coupled nonlinear diffusion equation and molecular rate equations. However, an unexpected experimental result was the observation of gain narrowing in samples that are smaller in size than the transport mean free path[3, 8], seemingly exposing an inadequacy of the usage of the diffusion approximation. Prasad et al[8] have shown that in this regime, the sub-mean-free-path scatterings, which are usually rare, are rendered important due to the high gain of the medium.

While simple, qualitative explanations have been put forth to explain the gross features of the phenomenon, there is, to date, no theory or model that accounts for the finer details. For example, based on the gain narrowing mechanism, one would merely expect a reduction in the threshold for linewidth collapse on the addition of particles, and no significant change in the emission profile, especially, in the peak position. However, experiments have shown, apart from a linewidth collapse at reduced thresholds, significant shifts in peak wavelengths. In addition, at high dye concentrations, some dye-scatterer systems have shown bichromatic emission and competition between the two modes[5, 6, 8]. Once again, attempts have been made to explain bichromaticity, analytically, within the diffusion approximation[9], and numerically, using Monte Carlo techniques for various models[6]. The excitation power dependent spectral shifts have also been investigated experimentally and theoretically[12]. It may be noted that all the hitherto proposed models tend to work within the diffusion regime, and have not been examined in the weak scattering regime.

We have performed experiments on a dye-scatterer system, chiefly with the aim of constructing a model that explains the typical observations. In an effort to explain these experimentally observed features, particularly the fact that these features are observed at $l^* > L$, and to explore the possibility of predicting the emission spectrum, we have proposed a simple model and carried out extensive Monte Carlo simulations based on it. Our simulations of several dye-scatterer systems over a range of dye concentrations, particle densities and pump intensities have enabled us to explain various reported features like threshold reduction, linewidth narrowing, shift in wavelength of peak emission and bichromaticity. Given the concentration and absorption and fluorescence spectra of the dye, our code can predict the shift in wavelength with increasing pump power and also the mode positions. Unlike the previous Monte Carlo treatment[11] which was restricted to $L > l^*$ and assumed isotropic scattering, we study the system at all three particle densities, $L > l^*$, $L \sim l^*$ and $L < l^*$, i.e., even outside the diffusion approximation. We also incorporate the wavelength dependence of the transport mean free path, and the

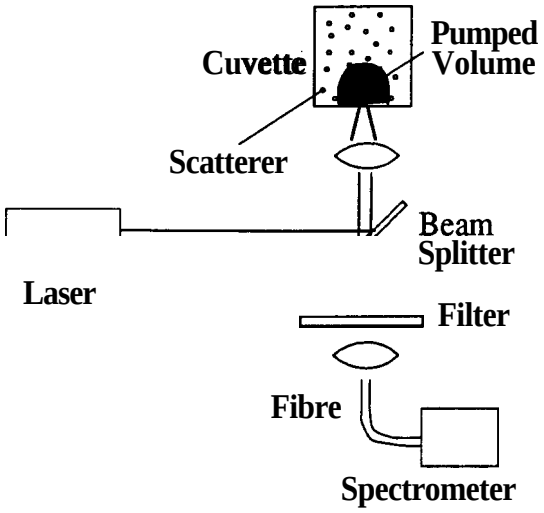

Figure 7.1: *Experimental setup for studying the emission spectrum from a random amplifying medium. Although the sample volume is about 1 cc, the excited volume is much lesser, and depends upon the dye concentration and pump beam energy.*

anisotropy of scattering explicitly by calculating the anisotropy parameter.

7.2 Experimental details

The system under study is a high efficiency dye solution, in which are suspended submicron sized monodisperse spherical dielectric scatterers. The dye is pumped by high intensity nanosecond pulses at a wavelength close to the maximum in its absorption profile, and the emission is studied as a function of dye concentration, number density of scatterers, and intensity of pump. The experimental setup used to study emissions from random amplifying media is as shown in Figure 7.1.

The scattering-amplifying medium consisted of the dye Rhodamine 590 perchlorate dissolved in de-ionised, triple distilled water with polystyrene microspheres of diameter 0.12μ (Seradyn Corporation) suspended in it. The dye concentration was varied from 5×10^{-5}M to 5×10^{-2}M. At each dye concentration, the scatterer density was increased from 10 $/cc$ to 1.24×10^{12} $/cc$ in decades. The dye-scatterer system is contained in a cuvette of size 1cm x 1cm x 1cm. Ten nanosecond wide pulses from a frequency doubled

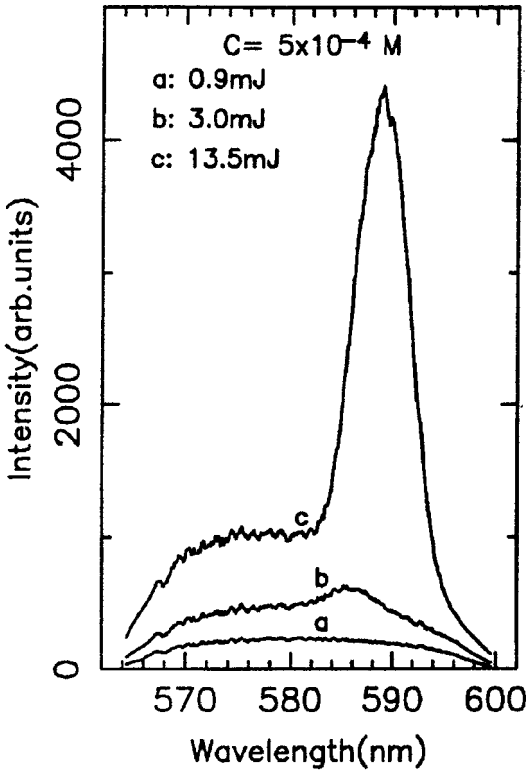

Figure 7.2: *Experimentally observed emission spectra, illustrating gain enhancement, obtained from the pure dye at a concentration of* $5 \times 10^{-4} M$, *at three different pump energies. Also note the shift in the wavelength of peak emission.*

(532nm) NdYAG laser at a repetitiion rate of 10 Hz are focussed onto the front face of the cuvette. Consequently, a restricted subvolume of the dye is pumped. The yellow-orange-red fluorescence is emitted in all directions. However, the light emitted from the front face alone is collected by a lens, and analysed on a spectrograph, in our case, a PC-based fibre-optic spectrometer (Ocean Optics).

7.3 Experimental results

We noted that no lasing action was observed at the low dye concentration (5×10^{-5}M) upto the scatterer density of 10^{12} /*cc* and the spectrum consisted of a weak, broad dye

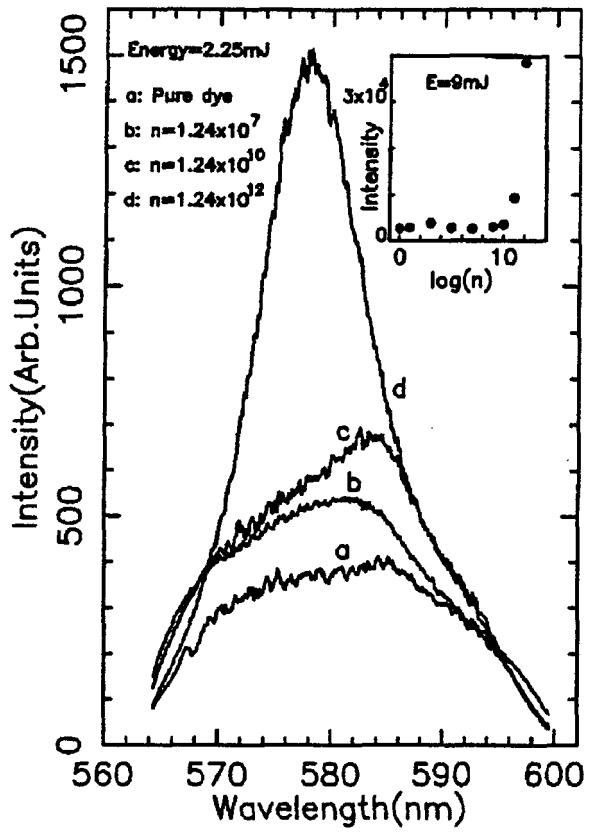

Figure **7.3:** *Experimentally observed emission spectra of the dye (5 x $10^{-4}M$) at various scatterer densities, at a pump energy of 2.25mJ. The inset shows the enhancement in emission as a function of scatterer density at a pump energy of 9 mJ.*

emission. Lasing like characteristics were observed in the dye of concentration 5×10^{-4}M, which we shall first present here. The figure **7.2** shows the emission spectra of the pure dye at three different pump energies.

At low pump energies, the pure dye showed broad emission of FWHM $\sim$ **30** nm, which narrowed to less than 6 nm, as the pump energy was increased beyond **3 mJ**. This is the amplified spontaneous emission. A reduction in the threshold pump energy as compared with that of a pure dye was observed when the density of scatterers exceeded 10^9 */cc.* Figure **7.3** shows the emission profiles for different scatterer densities at a fixed pump energy of **2.25 mJ**. While curves *a* and *b* correspond to the system below the threshold, curve *c* corresponds to the system close to the threshold. The inset in figure **7.3** shows

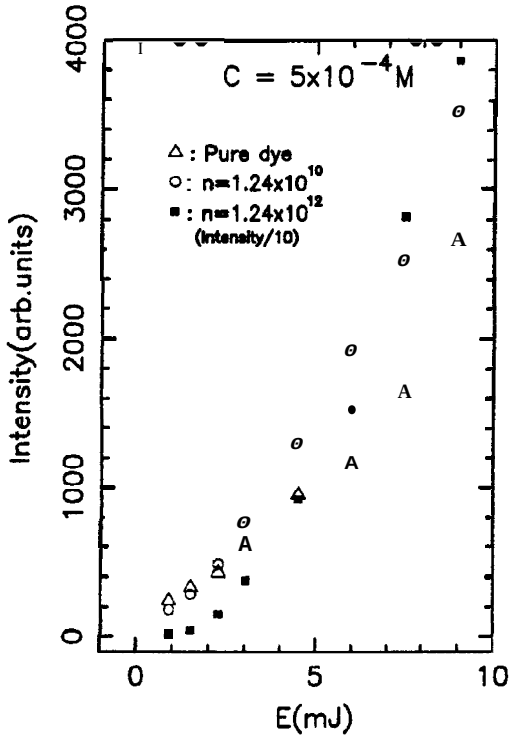

Figure *7.4: Peak intensity of emission, as seen from the experiments, illustrating gain enhancement, obtained from the pure dye at a concentration of* $5 \times 10^{-4} M$*, at three different scatterer densities. Note that, in the case of the scatterer concentration of 1.24* x $10^{12}/cc$*, the intensity has been divided by a factor of 10 to bring it to scale.*

the peak intensity as a function of scatterer density for a fixed pump energy of 9 mJ. Figures *7.4* and 7.5 show the peak intensity and the FWHM respectively as a function of input pump energy for pure dye and for different scatterer densities. It is clear from Figs *7.4 - 7.5* that the phenomenon of lasing action is seen even with n = *1.24* x $10^{10}/cc$, for which $l^* = 35$cm (for the central wavelength of the emission band), and clearly $l^* >> L$.

At the higher dye concentration $(5 \times 10^{-3}\mathrm{M})$, the pure dye showed an emission spectrum with two broad peaks A and B, centred at *578* nm and *620* nm respectively. This is similar to the bichromatic emission seen in higher dye concentrations, as reported earlier literature. In the presence of scatterers, at a density of n = *1.24* x $10^{12}/cc$, the relative intensities of the two peaks oscillated with increasing pump energy, as shown in figure *7.6.* At the highest pump energy, peak A grew at the expense of peak B, which can be seen

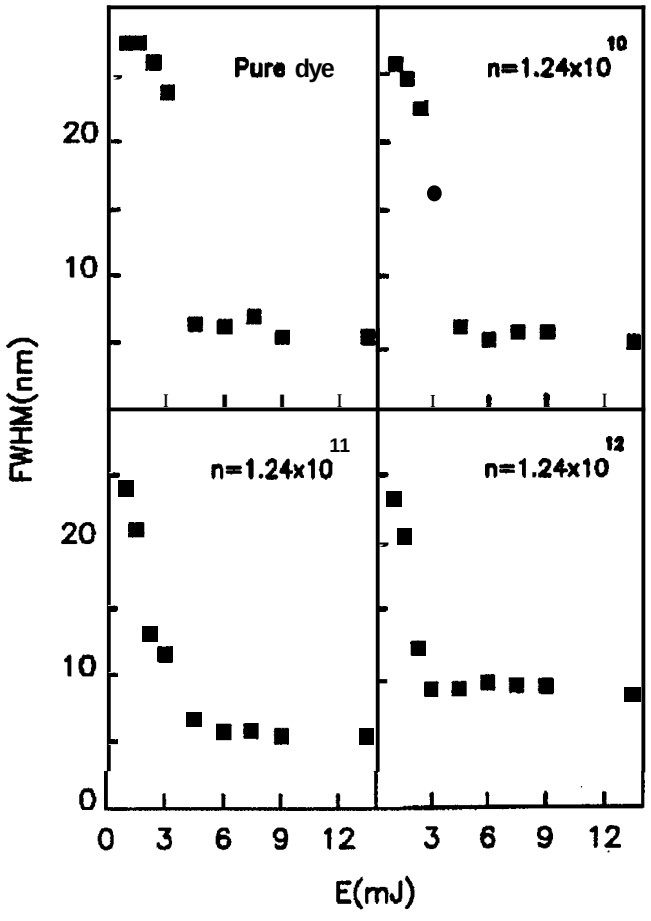

Figure *7.5: Experimentully observed behaviour of FWHM with pump energy for the pure dye and the dye with various scatterer densities.*

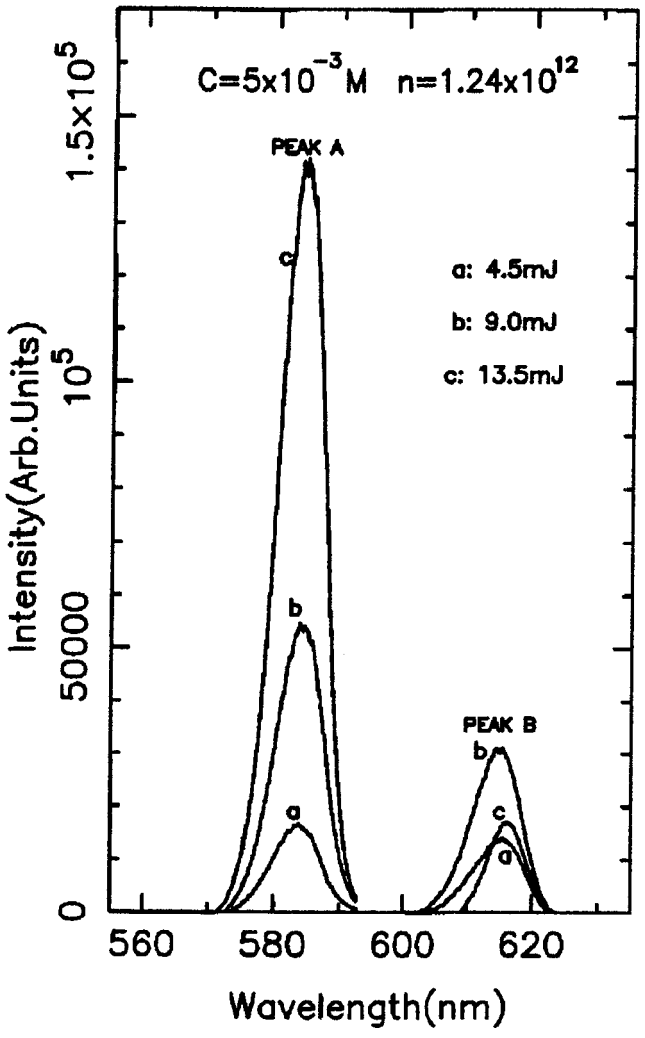

Figure **7.6:** *Bichromatic emission and mode competition seen experimentally from a dye at a concentration of* $5 \times 10^{-3} M$*, with a scatterer density* $1.24 \times 10^{12}/cc$.

by comparing curves b and c in figure **7.6.** Such a behaviour has been reported as mode competition in the earlier reports on random amplifying media.

These are the typical experimental observations relevant to randomised liquid amplifying media. It is of particular interest to note that lasing like characteristics are seen even with weak scattering, i.e., when $l^* >>$ L. Clearly, there is a need of a model which encompasses this fact, that subdiffusive scattering is also capable of creating enough feedback for lasing. The models based on the diffusion theory are incapable of doing so. Hence, we proceed to study the problem numerically through Monte Carlo simulations where we have a free handle on parameters like the strength of scattering, the dye concentration, the pump energy etc. We now describe the simulations.

7.4 Numerical simulations

Our simulations incorporate the same experimental setup. A cubical unit sample volume contains N dye molecules (where $N/\text{volume} = \text{C}$, the concentration of the dye), of which N_0 are in the ground state, and N_1 in the excited state. Each pump pulse of intensity I raises P molecules to the excited state. Thus, after each pump pulse, N_0 is decremented by P, and N_1 incremented by the same amount. Similarly, the population N_1 in the excited state is decremented by 1 and the population in the ground state is incremented by 1 on the emission of each photon. Let a dye molecule at some position (x, y, z), inside the pumped volume, (picked randomly from a uniform distribution), spontaneously emit a photon. The wavelength of the emitted photon is picked randomly from a uniform distribution weighted by the measured fluorescence spectrum of the dye, while the direction of travel is picked randomly from a uniform distribution over 4π steradians. The photon travels a distance 1 before being scattered. As in the chapter 5, the distance l is picked from an exponential distribution that is calculated as $l = -l_s \ln \sum$, where $\sum$ is a uniform variate $\in (0,1)$. This gives an exponential distribution for the scattering lengths with the mean as the scattering mean free path $l_s = 1/n_s\sigma_s$, where n_s is the scatterer density, and a, is the

scattering cross-section of the particles. The scattering cross-section is calculated from the Mie theory[13]. Thus, this distance 1, depends on the number density of scatterers and the size of the scatterer. Having travelled a distance 1, the photon is scattered, and now travels in a different direction (θ, ϕ) (referring to the direction of the incident photon as Z axis) for a distance 1'. The azimuthal angles ϕ after scattering are uniformly distributed over the range 0 to 2π radians as the scattering is cylindrically symmetric around the incident direction. The distribution of the scattering angles θ was given by the Henyey-Greenstein distribution[14], described by equation 5.9.

The process of propagation and scattering of the photon is repeated till it exits the sample volume. The total pathlength L that the photon travels is recorded. If it exits from the front face, this photon is taken into account for determining the emission spectrum. The wavelength λ had been randomly picked and weighted by the fluorescence spectrum, as described earlier. This photon is amplified by stimulated emission by a factor N_a=exp(αL), where a is the gain per unit length at that wavelength for the given concentration of the dye and the given pump energy and L is the total pathlength in the medium. Thus, the emission spectrum will contain N_a photons at wavelength λ due to one spontaneously emitted photon at λ. Irrespective of the face through which the photon exits, its amplification is calculated, as this has implications on the populations N_0 and N_1. The whole process of creation of a spontaneous photon, and the tracing of its path till it exits the medium is repeated 5 million times. The calculations are repeated for increasing pump intensities, i.e., increasing P.

The simulations were carried out for dye concentrations of 5 x 10^{-3}M and 3 x 10^{-2}M. The particles were taken to be 0.12μ diameter polystyrene spheres, with a refractive index of 1.5. For each dye concentration, the particle number density was varied from $10^{10}/cc$ to $10^{12}/cc$, i.e, the transport mean free path l^* varies from 7.5 cm to 0.75 mm for λ = 0.58 μ. [Henceforth in this chapter, l^* will always be mentioned for λ = 0.58 μ, which is approximately the centre of the emission band.]

7.5 The amplification factor

We assume that only the singlet manifold of the dye energy states participate in the emission process. A strong argument in favour of this supposition is that the intersystem crossing time from the singlet to the triplet manifold is much larger than the pulsewidths of the pump used in experiments which are ~5ns. (For example, the intersystem crossing time in Rhodamine 6G $\sim 0.6 \times 10^{-7}$sec[15]). Even though such intersystem crossings are statistically probable, the triplet emission and absorption spectra have a considerable overlap, forbidding any strong emission due to dipole transitions. Only the singlet absorption and emission cross-sections are used to calculate the gain of the spontaneously emitted photon.

The gain that is gathered by the photon is calculated as[16]

$$\alpha(\lambda) = \exp[(\sigma_{se}(\lambda)N_1 - \sigma_{abs}(\lambda)N_0)L] \tag{7.1}$$

where N_1 and N_0 are the excited state and ground state occupation numbers, respectively, and L is the total pathlength of the photon in the medium. $\sigma_{abs}(\lambda)$ is the absorption cross-section , and $\sigma_{se}(\lambda)$ is the stimulated emission cross-section at the wavelength A.

The stimulated emission cross-section at a wavelength λ is given by[16]

$$\sigma_{se}(\lambda) = \frac{\lambda^2}{8\pi}\frac{Q(\lambda)}{\phi_f} \tag{7.2}$$

where ϕ_f is the fluorescence efficiency of the dye, and $Q(\lambda)$ is the number of fluorescence quanta at the wavelength λ emitted per second per excited dye molecule.

7.6 Simulation results

We first show that our simulations reproduce the experimental results quite well. Figure 7.7 gives the emission spectra of the pure dye at the concentration of 5×10^{-3}M at various pump intensities, as observed in the simulations. Starting from a 20 nm wide emission spectrum at a pump power of –0.2 mJ, the emission narrows down to –6 nm at

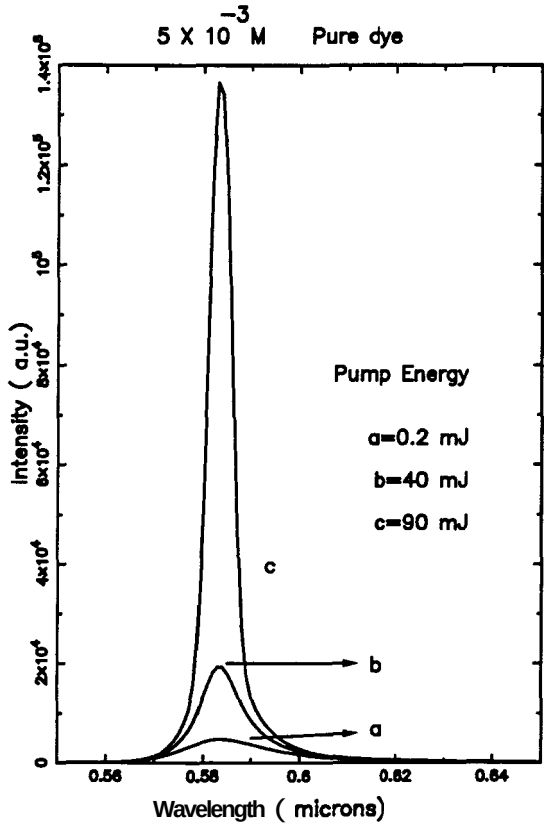

Figure 7.7: *Emission spectrum of the pure dye at a concentration of 5 x* $10^{-3}M$*, at three different pump energies, as seen from the simulations.*

a pump power of 90 mJ. The wavelength of peak emission is λ_{max}, and the emission is in a single mode. This is consistent with the experimentally observed line narrowing in the pure dye at high pump powers[8]. Figure 7.2 shows the experimentally observed spectra of the pure dye at three different pump energies. The emission intensity is clearly seen to be enhanced at a wavelength $\sim 585nm$.

As mentioned earlier, characteristics like linewidth narrowing and gain enhancement have been observed in disordered amplifying media at various degrees of scattering. We examined each one, by altering the number of scatterers in the simulated volume, and found clear agreement of our inferences with the experimental data. We present our results as follows. Figures 7.8, 7.9 and 7.10 give the emission spectrum, as obtained from our simulations, of the sample consisting of the dye at a concentration of 5 $\mathbf{x10^{-3}}$M with

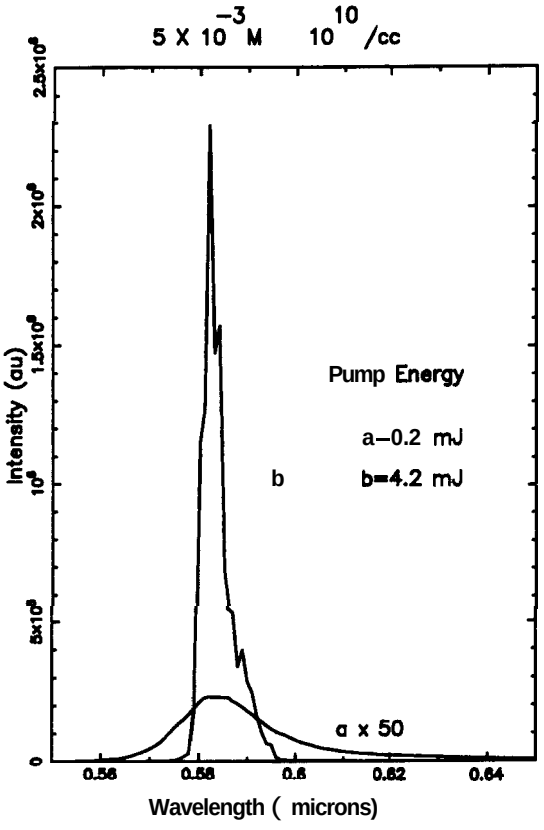

Figure *7.8: Emission spectrum of the dye* ($5 \times 10^{-3} M$) *with a scatterer density of* $10^{10}/cc$ ($l^* = 7.5$ *cm), as obtained from the numerical simulations. The scattering is weak, in the sub-diffusion regime, since* $L < l^*$. *The profile (a) is scaled up by a factor of 50. Threshold reduction is evident on comparison of the magnitude of the pump energy here with that illustrated in Figure* **7.7.**

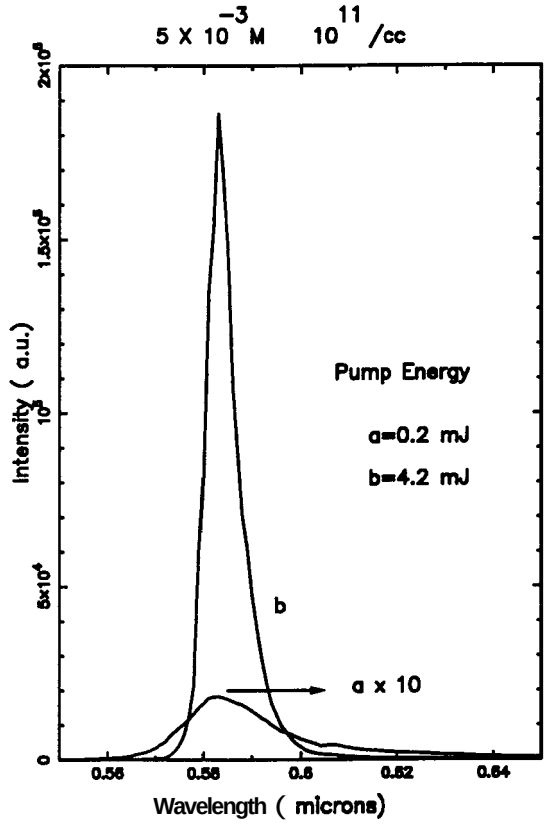

Figure 7.9: *Emission spectrum of the dye ($5 \times 10^{-3} M$) with a scatterer density of $10^{11}/cc$ ($l^* = 7.5$ mrn) as observed from numerical simulations. The profile (a) is scaled up by a factor of 10.*

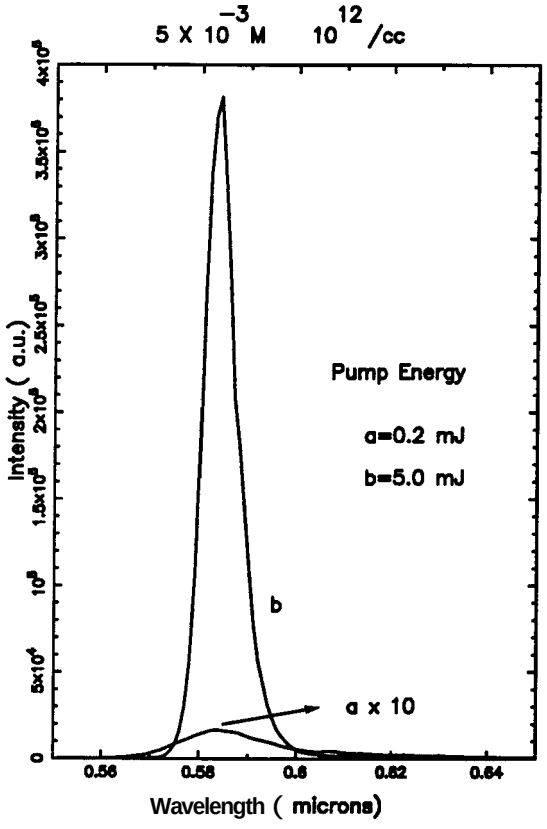

Figure 7.10: *Emission spectrum of the dye ($5 \times 10^{-3} M$) with a scatterer density of $10^{12}/cc$ ($l^* = 0.75$ mm) as observed from numerical simulations. The scattering is well within the diffusion regime. The profile (a) is scaled up by a factor of 10.*

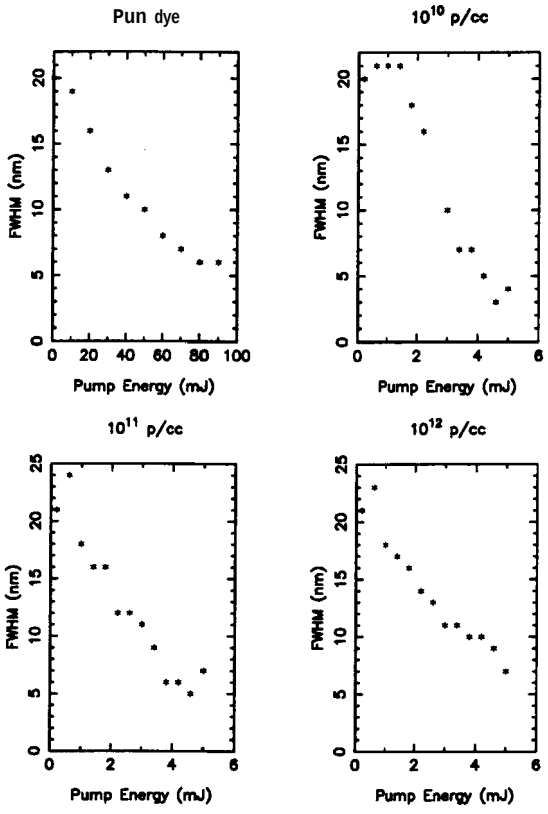

Figure 7.11: *The variation of FWHM with pump energy for the pure dye and the dye with various scatterer densities, as obtained from our simulations.*

scatterers of number densities 10^{10} $/cc$ ($l^* = 7.5$ cm), 10^{11} $/cc$ ($l^* = 7.5$ mm) and $10^{12}/cc$ ($l^* = 0.75$ mm). The fact that our system width L was 1 cm shows that we have examined three different cases *viz.*, L $< l^*$, L $\sim l^*$,and L $>$ I*. The addition of particles leads to a dramatic increase in the peak intensity at very low pump powers, as is obvious from the figures.

Figure 7.11 shows the variation of the full width at half maximum with pump power in the above four cases. It is seen that upon the addition of scatterers, the reduction in FWHM occurs at much lower pump powers (thresholds) than that in the case of the pure dye. The threshold is brought down by a factor of about 10. As compared to the case of the pure dye where the threshold occurs at 15 mJ, it is observed at 1.5 mJ at a particle density of 10^{10} $/cc$ (I*$= 7.5$cm), and at 0.5 mJ at a density of 10^{12} $/cc$ (I*$= 0.75$mm). It

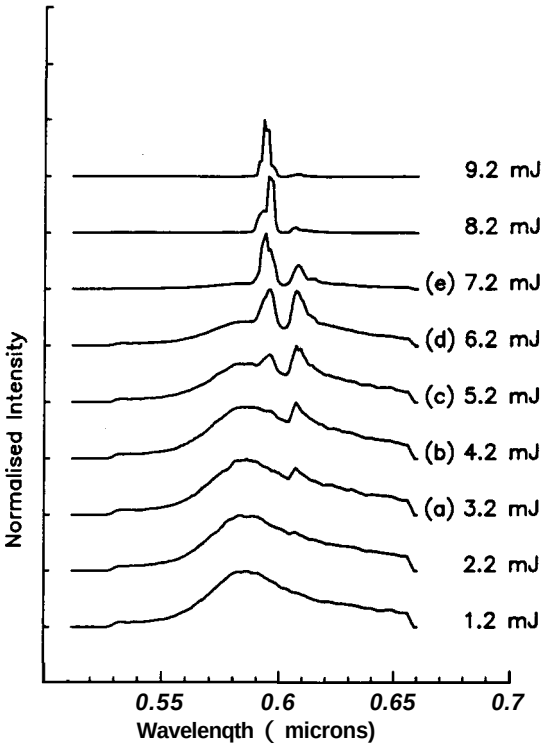

Figure 7.12: *Bichromatic emission from a dye at a concentration of* $3 \times 10^{-2} M$, *with* a *scatterer density* $10^{10}/cc$ ($l^* = 7.5$ *cm) as observed from the simulations. Normalised emission spectra are shown with the corresponding pump energies alongside.*

is evident that even in the so called weak scattering regime, the high gain of the medium suffices to narrow the spectral line considerably. Further, the threshold is seen to lower with increasing particle density. All these features, *viz.*, the behaviour of the FWHM, line narrowing due to sub-mean-free-path scatterings and threshold reduction with increasing particle density are in fair agreement with reported experiments.

Another experimentally observed feature is the bichromatic emission and the competition between the two modes. At high dye concentrations, the emission is seen to have two peaks, at wavelengths that vary from dye to dye. We call these the yellow and the red modes, with the red being the one at the longer wavelength. The results of our simulations for a dye of concentration 3×10^{-2} M and a scatterer density of 10^{10} $/cc$ ($l^* = 7.5$ cm) are given in Figure 7.12.

The figure shows the normalised emission spectra at various pump energies, while the

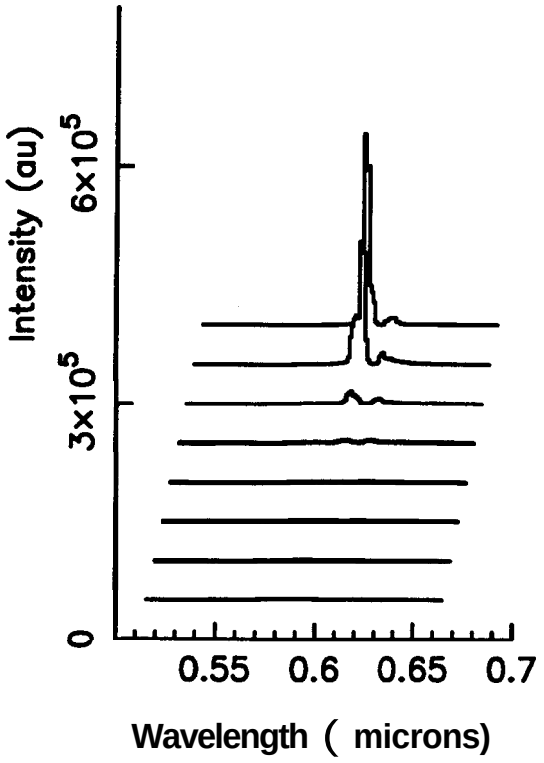

Figure 7.13: *The figure shows the spectra of figure 7.12, with the intensity at arbitrary units.*

figure 7.13 shows the same spectra with the peak intensities at arbitrary units. At low pump powers, the emission consists of a broad hump, peaked at 585 nm (yellow), with a small shoulder at 610 nm (red). On increasing the pump power, the shoulder is seen to grow quite rapidly, developing into a well defined, narrow peak, overtaking the other (yellow) mode in height (Fig 7.12b). On increasing the pump even further, the yellow mode also narrows (Fig 7.12c). At yet higher pump intensities, the yellow mode gains faster in intensity (Fig 7.12d), rising above the red mode (Fig 7.12 e). Eventually, the yellow mode narrows down to 5nm at the cost of the red mode. Figure 7.13 illustrates the variation in the energy of the two modes with increasing pump energy.

This is the competition between the two modes, discussed by various groups[5, 8]. It can also be seen, both from our simulations and reported experiments[5, 12], that the yellow peak has shifted from 585 nm to 590 nm.

It may be noted that, at the lower concentration, only the yellow mode lases, while, at high concentrations, mode competition is observed. This has been particularly emphasised in previously reported experiments[4, 8], and is clear upon comparing the experimental results in figures **7.3** and 7.6.

In order to understand the origin of this mode competition and the shift in the wavelength, we have studied, by numerical simulations, this phenomenon, over a wide range of number density of scatterers, dye concentrations, and dye systems. We arrived at the following explanation :

At low pump intensities, the emission is according to the fluorescence spectrum of the dye, with the emission maximum in the yellow (Fig 7.12). Though there is emission in the red, it is quite weak, and no peak in the red is discernible. As the pump power is increased, the peak in the red begins to develop. The dye molecules continue to emit according to the same fluorescence profile, as earlier. However, because of the significant overlap in the absorption and emission spectra of the dye in the yellow, a portion of the emission is reabsorbed by the dye. The absorption, however, being almost nil in the red, the red region gains more rapidly than the yellow. (Fig 7.12b, c). At higher pump powers, the dye is saturated by the pump photons, and thus absorption in the yellow is inhibited. Now once again the yellow peak dominates (Fig 7.12e). Finally, at higher pump powers, the dye lases at the wavelength where the difference between the emission cross-section and absorption cross-section is maximum. To verify this hypothesis, in the Monte Carlo simulations, we changed the absorption spectrum of the dye from its natural one, to one where absorption was zero for all wavelengths greater than 580nm. In this case, as expected, the yellow peak (590 nm) was more prominent all through, and the red peak was negligible.

7.7 Stimulated emission and self-absorption

We examine the emission of the pure dye with different concentrations and the dye with randomly placed scatterers separately. This enables us to address the question as to

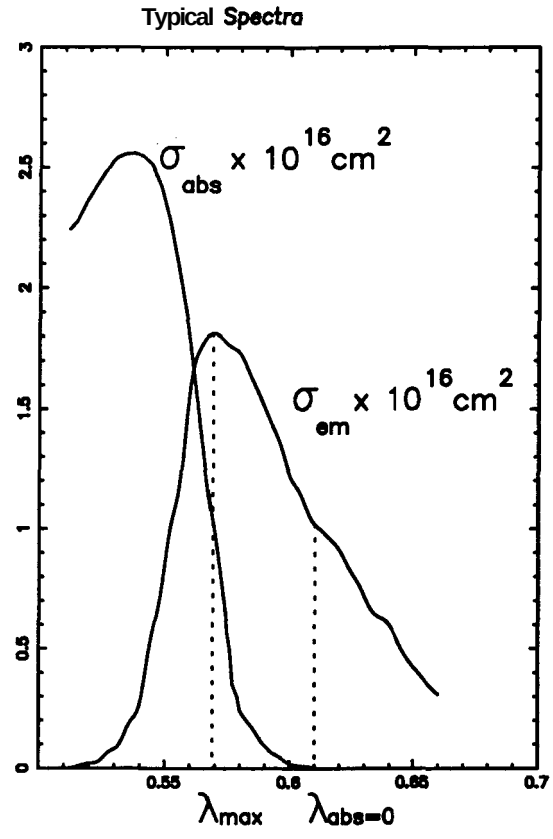

Figure **7.14:** *Typical absorption and emission spectra of a fluorescent dye, that form inputs to the simulation, showing the wavelength of peak emission and the wavelength at which the absorption goes to zero.*

why the emission is single mode at low dye concentrations and bichromatic at high dye concentrations.

We begin by noting that the dyes have a broad absorption spectrum, with the peak absorption in the green and the absorption spectrum extending deep into the fluorescence spectrum. Typical dye absorption and fluorescence spectra, that form inputs to our simulations, are shown in figure **7.14.**

Emitted light at wavelengths within this overlap region suffer from absorption by the ground state molecules of the dye. At low pump intensities, where nonlinear effects are unimportant, the dye emits according to the broadband fluorescence spectrum, with the emission maximum at some wavelength λ_{max}. At low concentrations, there are fewer

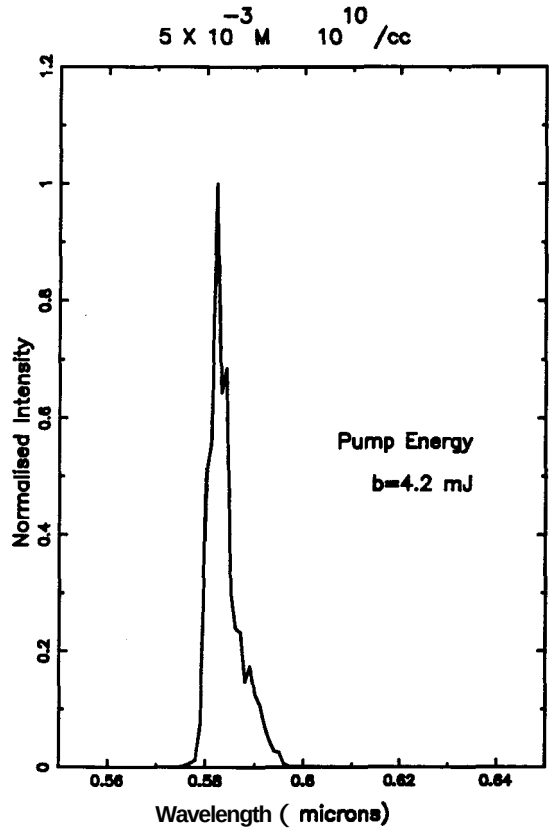

Figure 7.15: The *normalised emission spectrum at low dye concentration* ($5 \times 10^{-3} M$) *as obtained from the simulation.*

ground-state molecules. Consequently, the dye is easily bleached and the paucity of the ground state molecules facilitates stimulated emission rather than absorption. Since stimulated emission is maximum at A, the spontaneous fluorescence at the red wavelengths is suppressed, and the emission narrows to the A The emission is primarily single mode, as only the yellow mode is observed (Fig. 7.15). Figure 7.7 also shows this situation.

At higher dye concentrations, however, there is an abundance of ground state molecules that absorb the energy in the yellow mode. The red emission, however, passes relatively unhindered, and the spectrum appears to peak at two wavelengths. The positions of the two peaks depend upon the overlap of the absorption and emission spectra. As can be seen from figure 7.12, the yellow mode is seen to appear at or near the λ_{max}. From our simulations, we find that, at high pump powers, the yellow mode peaks not at A

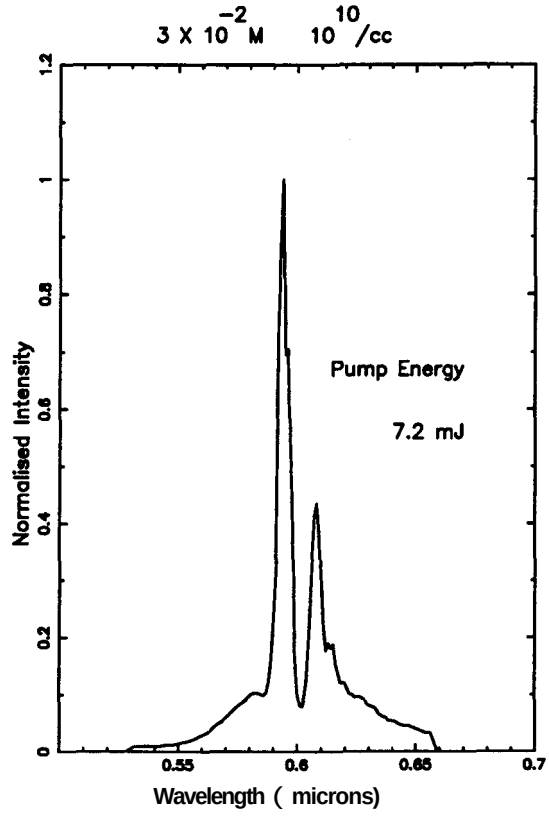

Figure 7.16: *The normalised emission spectrum at a higher dye concentration* $(3 \times 10^{-2} M)$ *as obtained from the simulation.*

but at the wavelength where the difference between the absorption and emission curves is maximum. This usually is close to, but not exactly at λ. This could be the basis of the shift of the wavelength of peak emission. The red mode develops at the wavelength where the absorption goes to zero, $\lambda_{abs=0}$ (Fig 7.16). The width of the red mode is dependent on the slope of the emission spectrum at $\lambda_{abs=0}$. Larger the slope, narrower is the red mode.

The addition of particles has a two-fold effect on the fluorescence process. Scattering of the photons within the active subvolume increases the pathlength of the photons, and increases the gain of the photon according to the equation 7.1. Further, the emission in the active subvolume is scattered out of it into the neighbouring unpumped dye region, resulting in the formation of a buffer subvolume. This is illustrated in the figure 7.17. The activity of this buffer depends upon the concentration of the dye and drastically affects

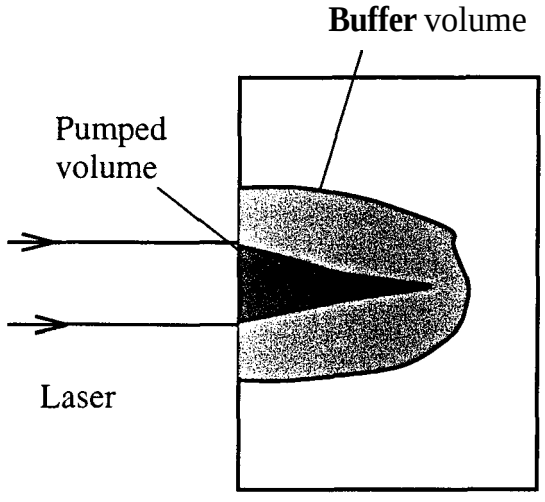

Figure 7.17: *Schematic elucidating the formation of a buffer volume surrounding the primary pumped volume in an amplifying medium. The size of the buffer depends upon the pump energy, concentration of the dye and the scatterer concentration. The activity of the buffer determines the spectral profile of the emission from the medium.*

the emission characteristics.

At low concentrations, the buffer, too, gets easily bleached, and contributes more excited state molecules for the stimulated emission. Self-absorption is weak because of absence of ground state molecules. The increased pathlengths of the photons enhance the stimulated emission greatly, and results into the dramatic reduction of the threshold.

At high concentrations, however, the buffer supplies more ground state molecules. So, the yellow emission is absorbed, inhibiting the stimulated emission. The red spontaneous emission from the buffer adds to that from the active subvolume, and the red peak observed is stronger than the yellow peak. As the pump intensity is increased, the buffer starts getting bleached. Consequently, the yellow mode starts growing at the cost of the red mode, and eventually narrows down. This has been observed experimentally as the mode competition at high concentrations.

A similar approach of the formation of a surrounding volume was put forth by Balachandran and Lawandy[6], where they consider that the surrounding volume absorbs the emission from the pumped volume at the lower wavelength (in their case, 617 nm) and

emits at the higher wavelength (648 nm). This model does not explain the dependence of the bichromaticity on the concentration of the dye, neither does it elucidate the reasons for the competition seen between the modes with increasing pump energy. Our model differs from theirs in that, in our case, the activity of the buffer subvolume depends upon the concentration of the dye and also the pump intensity. Thus it shows the observed mode competition as explained above.

The spectral shift was investigated recently by Totsuka et al[12], using the saturation absorption in the excitation process. They limited the study of their model to low concentration dyes, and thus could not observe bichromaticity that is seen at higher dye concentrations.

It can thus be concluded that the characteristics of the dye emission primarily depend upon the nature and overlap between the absorption and emission spectra. The addition of particles increases the pathlength of the photons within the active subvolume and creates an active buffer subvolume around it. The rapidity of narrowing depends upon the increased pathlengths and the change in the spectral profile depends upon the activity of the buffer.

7.8 Conclusions

In this chapter, we have reported our investigations of the emissions from random liquid amplifying media. Experimental observations obtained from a dye-scatterer system involving the laser dye, Rhodamine 6G, and polystyrene microparticles, were used as the basis to develop a model for the spectral features of the emissions from such media. We have examined the phenomena of line-narrowing and bichromatic emission in random amplifying media through extensive experiments, followed by extensive Monte Carlo simulations. We explain the various reported experimental features through a model that includes only the stimulated emission and self-absorption of photons performing a three dimensional random walk inside the amplifying medium. We present the results for all three regimes

of scattering, $L < \ell^*$, $L \sim l^*$ and $L > l^*$. We discuss various processes, *viz* stimulated emission, self-absorption, formation of a secondary excited region involved in the phenomenon of lasing, and their dependence on external variables like the pump energy, concentration of the dye, strength of scattering etc. The shift in wavelength of maximum emission, bichromatic emission and the competition between modes have been explained. Finally, we underline the importance of the profile of fluorescence spectrum and the absorption spectrum of the amplifying material in deciding the profile of the random laser emission above threshold.

Bibliography

[1] V. S. Letokhov, Sov. Phys. JETP 26, 835 (1968).

[2] V. M. Markushev, V. F. Zolin and C. M. Briskina, Sov.J.Quantum Electron. 16, 281 (1986).

[3] N. M. Lawandy, R. M. Balachandran, A. S. L. Gomes and E. Sauvain, Nature 368, 436 (1994).

[4] W. L. Sha, C. H. Liu and R. R. Alfano, Optics Letters 19, 23 (1994).

[5] W. L. Sha, C. H. Liu, Feng Liu and R. R. Alfano, Optics Letters 21, 16 (1996).

[6] R. M. Balachandra'n and N. M. Lawandy, Optics Letters 21, 19 (1996)

[7] R. M. Balachandran, D. Pacheco and N. M. Lawandy, App. Opt. 35, 4 (1996).

[8] B. Raghavendra Prasad, Hema Ramachandran, Ajay Kumar Sood , C. K. Subramanian, N. Kumar, App. Opt. 36, 30 (1997).

[9] Sajeev John and Gendi Pang, Phys. Rev. A 54, 3642 (1996).

[10] Diederik Wiersma and Ad Lagendijk, Phys. Rev. E 54 , 4256 (1996).

[11] G. A. Berger, M. Kempe and A. Z. Genack, Phys. Rev. E 56, 6118 (1997).

[12] K. Totsuka, M. A. I. Talukder, M. Matsumoto and M. Tomita, Phys. Rev. B 59, 50 (1999).

[13] H. C. van de Hulst, Light Scattering by Small Particles, (Dover, New York, 1981).

[14] L. C. Henyey and J. L. Greenstein, Astrophys.J. 93, 70 (1941).

[15] B. B. Snavely, Dye Lasers, (Springer-Verlag, Berlin, 1973).

[16] F. P. Schafer, Dye Lasers, (Springer-Verlag, Berlin,1973).